A Subgridding Technique for the CIP Method

Yoshiaki Ando
Graduate School of Informatics and Engineering
The University of Electro-Communications
Chofu, Tokyo 182-8585
Email: y-ando@uec.ac.jp

Takashi Hirota
Simulatio Co. Ltd.
Yokohama, Japan

***Abstract*—In this study, we propose a subgridding technique in the constrained interpolation profile (CIP) method in order to simulate electromagnetic fields in the presence of objects with fine structures. The subgridding technique consists of spatial and temporal interpolations at the interface between main coarse grids and local fine grids. In the present study, we consider a two-dimensional problem with TM_z polarization. In order to examine the validation of the proposed method, spatial and temporal interpolation schemes are implemented separately. The numerical results show that both the interpolation schemes operate successfully, and the relative errors are extremely small in wide frequency band.**

I. Introduction

The constrained interpolation profile (CIP) method has been developed to analyze multi-phase problems[1], and applied to electromagnetic problems successfully. Various techniques for solving electromagnetic field problems have been reported, e.g. the perfectly matched layer[2], the total-field/scattered field boundary[3], etc.

Numerical methods based on the finite-difference[4], or the finite element methods have the nature in which the computational costs increase with finer grids used. The subgridding technique allows us to analyze fine structures with relatively low computational costs. It uses the local sub-grid region which has smaller cells than the main grids, and we can localize the finer grids region to decrease the computational burden. Although the unstructured grids technique for the CIP method has been developed as the Soroban grids[5], it does not localize the region with the small times step, and it losts the advantage.

In this study, we propose the subgridding technique for the CIP method. Xiao et al.[6] proposed the separate boundaries where the temporal and the spatial interpolations are used, and we use the concept in this study.

II. The CIP method for 2-D TM_z EM simulation

Consider electromagnetic fields of TM_z waves in the free space (the permittivity and the permeability are ε_0 [F/m] and μ_0 [H/m], respectively). Here we introduce normalized field variables e_z, h_x, and h_y:

$$e_z = \sqrt{\varepsilon_0}E_z, \quad h_x = \sqrt{\mu_0}H_x, \quad \text{and} \ \ h_y = \sqrt{\mu_0}H_y, \quad (1)$$

where E_z, H_x, and H_y are the usual electric and mangetic fields in [V/m] and [A/m], respectively. The Maxwell equations are written in the matrix form:

$$\frac{\partial}{\partial t}\begin{bmatrix} e_z \\ h_x \\ h_y \end{bmatrix} + \frac{\partial}{\partial x}\begin{bmatrix} 0 & 0 & -c_0 \\ 0 & 0 & 0 \\ -c_0 & 0 & 0 \end{bmatrix} \bullet \begin{bmatrix} e_z \\ h_x \\ h_y \end{bmatrix} + \frac{\partial}{\partial y}\begin{bmatrix} 0 & c_0 & 0 \\ c_0 & 0 & 0 \\ 0 & 0 & 0 \end{bmatrix} \bullet \begin{bmatrix} e_z \\ h_x \\ h_y \end{bmatrix} = \mathbf{0}, \quad (2)$$

where c_0 is the speed of light in vacuum.

Applying the directional splitting technique to the Eq. (2), we have two equations corresponding to the advection in the x- and the y-directions, as follows.

$$\frac{\partial}{\partial t}\begin{bmatrix} e_z \\ h_y \end{bmatrix} + \frac{\partial}{\partial x}\begin{bmatrix} 0 & -c_0 \\ -c_0 & 0 \end{bmatrix} \bullet \begin{bmatrix} e_z \\ h_y \end{bmatrix} = \mathbf{0}, \quad (3)$$

$$\frac{\partial}{\partial t}\begin{bmatrix} e_z \\ h_x \end{bmatrix} + \frac{\partial}{\partial y}\begin{bmatrix} 0 & c_0 \\ c_0 & 0 \end{bmatrix} \bullet \begin{bmatrix} e_z \\ h_x \end{bmatrix} = \mathbf{0}, \quad (4)$$

Diagonalizing the matrices including c_0 gives

$$\frac{\partial}{\partial t}\begin{bmatrix} f_x^+ \\ f_x^- \end{bmatrix} + \frac{\partial}{\partial x}\begin{bmatrix} c_0 & 0 \\ 0 & -c_0 \end{bmatrix} \bullet \begin{bmatrix} f_x^+ \\ f_x^- \end{bmatrix} = \mathbf{0}, \quad (5)$$

$$\frac{\partial}{\partial t}\begin{bmatrix} f_y^+ \\ f_y^- \end{bmatrix} + \frac{\partial}{\partial y}\begin{bmatrix} c_0 & 0 \\ 0 & -c_0 \end{bmatrix} \bullet \begin{bmatrix} f_y^+ \\ f_y^- \end{bmatrix} = \mathbf{0}, \quad (6)$$

where $f_x^\pm$ and $f_y^\pm$ stand for $e_z \mp h_y$ and $\pm e_z + h_x$, respectively.

The CIP method can be used to solve the above advection equations:

$$\begin{aligned} f_x^{\pm,*}(i,j) &= A_{x1}^{\pm,t} f_x^{\pm,n}(i,j) + A_{x2}^{\pm,t} f_x^{\pm,n}(i \mp 1, j) \\ &\quad + A_{x3}^{\pm,t} g_x^{\pm,n}(i,j) + A_{x4}^{\pm,t} g_x^{\pm,n}(i \mp 1, j) \quad (7) \\ g_x^{\pm,*}(i,j) &= B_{x1}^{\pm,t} g_x^{\pm,n}(i,j) + B_{x2}^{\pm,t} g_x^{\pm,n}(i \mp 1, j) \\ &\quad + B_{x3}^{\pm,t} f_x^{\pm,n}(i,j) + B_{x4}^{\pm,t} f_x^{\pm,n}(i \mp 1, j) \quad (8) \\ \eta_x^{\pm,*}(i,j) &= C_{x1}^{\pm,t} \eta_x^{\pm,n}(i,j) + C_{x2}^{\pm,t} \eta_x^{\pm,n}(i \mp 1, j) \quad (9) \end{aligned}$$

$$\begin{aligned} f_y^{\pm,*}(i,j) &= \frac{1}{2}(f_y^{+,n} + f_y^{-,n}) \pm \frac{1}{2}(f_x^{+,*} + f_x^{-,*}) \quad (10) \\ g_y^{\pm,*}(i,j) &= \frac{1}{2}(g_y^{+,n} + g_y^{-,n}) \pm \frac{1}{2}(\eta_x^{+,*} + \eta_x^{-,*}) \quad (11) \\ \eta_y^{\pm,*}(i,j) &= \frac{1}{2}(\eta_y^{+,n} + \eta_y^{-,n}) \pm \frac{1}{2}(g_x^{+,*} + g_x^{-,*}) \quad (12) \end{aligned}$$

$$\begin{aligned} f_y^{\pm,n+1}(i,j) &= A_{x1}^{\pm,t} f_y^{\pm,*}(i,j) + A_{x2}^{\pm,t} f_y^{\pm,*}(i, j \mp 1) \\ &\quad + A_{x3}^{\pm,t} g_y^{\pm,*}(i,j) + A_{x4}^{\pm,t} g_y^{\pm,*}(i, j \mp 1) \quad (13) \\ g_y^{\pm,n+1}(i,j) &= B_{x1}^{\pm,t} g_y^{\pm,*}(i,j) + B_{x2}^{\pm,t} g_y^{\pm,*}(i, j \mp 1) \\ &\quad + B_{x3}^{\pm,t} f_y^{\pm,*}(i,j) + B_{x4}^{\pm,t} f_y^{\pm,*}(i, j \mp 1) \quad (14) \\ \eta_y^{\pm,n+1}(i,j) &= C_{x1}^{\pm,t} \eta_y^{\pm,*}(i,j) + C_{x2}^{\pm,t} \eta_y^{\pm,*}(i, j \mp 1) \quad (15) \end{aligned}$$

$$f_x^{\pm,n+1}(i,j)=\frac{1}{2}(f_y^{+,n+1}-f_y^{-,n+1})\mp\frac{1}{2}(f_x^{+,*}+f_x^{-,*}) \quad (16)$$

$$g_x^{\pm,n+1}(i,j)=\frac{1}{2}(\eta_y^{+,n+1}-\eta_y^{-,n+1})\mp\frac{1}{2}(g_x^{+,*}+g_x^{-,*}) \quad (17)$$

$$\eta_x^{\pm,n+1}(i,j)=\frac{1}{2}(g_y^{+,n+1}-g_y^{-,n+1})\mp\frac{1}{2}(\eta_x^{+,*}+\eta_x^{-,*}) \quad (18)$$

where $g_x^{\pm}$, $\eta_x^{\pm}$, $g_y^{\pm}$, and $\eta_y^{\pm}$ are $\frac{\partial}{\partial x}f_x^{\pm}$, $\frac{\partial}{\partial y}f_x^{\pm}$, $\frac{\partial}{\partial y}f_y^{\pm}$, and $\frac{\partial}{\partial x}f_y^{\pm}$, respectively.

III. The subgrid technique for the CIP method

The subgrid technique consists of the temporal and the spatial interpolations between the main and the local grids. In this section, we develop them separately.

A. The spatial interpolation technique

Suppose the main and the local grids are located as shown in Fig. 1. Here we consider the mesh ratio 2.

At the interface between the main and the local grids the profiles cannot be interpolated because the neighbouring grids in the upwind direction do not exist. In this study, we use the average values at the neighbouring main grids. Therefore, the updating equations are given by

$$\begin{aligned} f_{s,x}^{+,*}(1,2k) &= A_{x1}^{+}f_{s,x}^{+,n}(1,2k) \\ &+\frac{1}{2}A_{x2}^{+}\left\{f_{m,x}^{+,n}(i_1-1,j)+f_{m,x}^{+,n}(i_1-1,j+1)\right\} \\ &+A_{x3}^{+}g_{s,x}^{+,n}(1,2k) \\ &+\frac{1}{2}A_{x4}^{+}\left\{g_{m,x}^{+,n}(i_1-1,j)+g_{m,x}^{+,n}(i_1-1,j+1)\right\} \quad (19) \\ g_{s,x}^{+,*}(1,2k) &= B_{x1}^{+}g_{s,x}^{+,n}(1,2k) \\ &+\frac{1}{2}B_{x2}^{+}\left\{g_{m,x}^{+,n}(i_1-1,j)+g_{m,x}^{+,n}(i_1-1,j+1)\right\} \\ &+B_{x3}^{+}f_{s,x}^{+,n}(1,2k) \\ &+\frac{1}{2}B_{x4}^{+}\left\{f_{m,x}^{+,n}(i_1-1,j)+f_{m,x}^{+,n}(i_1-1,j+1)\right\} \quad (20) \\ \eta_{s,x}^{+,*}(1,2k) &= C_{x1}^{+}\eta_{s,x}^{+,n}(1,2k) \\ &+\frac{1}{2}C_{x2}^{+}\left\{\eta_{m,x}^{+,n}(i_1-1,j)+\eta_{m,x}^{+,n}(i_1-1,j+1)\right\} \quad (21) \end{aligned}$$

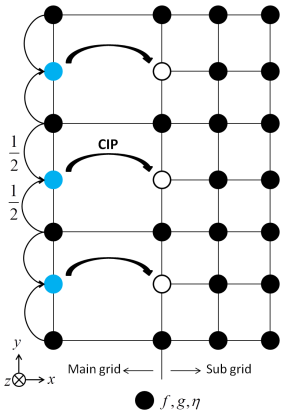

Fig. 1. The main and the local grids

$$\begin{aligned} f_{s,x}^{-,*}(NX_s,2k) &= A_{x1}^{-}f_{s,x}^{-,n}(NX_s,2k) \\ &+\frac{1}{2}A_{x2}^{-}\left\{f_{m,x}^{-,n}(i_2+1,j)+f_{m,x}^{-,n}(i_2+1,j+1)\right\} \\ &+A_{x3}^{-}g_{s,x}^{-,n}(NX_s,2k) \\ &+\frac{1}{2}A_{x4}^{-}\left\{g_{m,x}^{-,n}(i_2+1,j)+g_{m,x}^{-,n}(i_2+1,j+1)\right\} \quad (22) \\ g_{s,x}^{-,*}(NX_s,2k) &= B_{x1}^{-}g_{s,x}^{-,n}(NX_s,2k) \\ &+\frac{1}{2}B_{x2}^{-}\left\{g_{m,x}^{-,n}(i_2+1,j)+g_{m,x}^{-,n}(i_2+1,j+1)\right\} \\ &+B_{x3}^{-}f_{s,x}^{-,n}(NX_s,2k) \\ &+\frac{1}{2}B_{x4}^{-}\left\{f_{m,x}^{-,n}(i_2+1,j)+f_{m,x}^{-,n}(i_2+1,j+1)\right\} \quad (23) \\ \eta_{s,x}^{-,*}(NX_s,2k) &= C_{x1}^{-}\eta_{s,x}^{-,n}(NX_s,2k) \\ &+\frac{1}{2}C_{x2}^{-}\left\{\eta_{m,x}^{-,n}(i_2+1,j)+\eta_{m,x}^{-,n}(i_2+1,j+1)\right\} \quad (24) \end{aligned}$$

where k,l are the indeces, and $NX_s=2(i_2-i_1)+1, NY_s=2(j_2-j_1)+1$. The subscripts, m,s, stand for the variables belonging to the main and the local grids. The discretized coordinates are represented by (i,j) and (i_s,j_s) in the main and the local grids, respectively, and their relations are given by $i_s=2(i-i_1)+1, j_s=2(j-j_1)+1$ as shown in Fig. 2.

B. The temporal interpolation technique

The temporal interpolation realizes the different time step updating in a region from another. Here we call the region where computation is performed in the large time step ΔT, as "MG", and the one with the small time step $\Delta t=\frac{1}{2}\Delta T$, as "LG".

At the interface between MG and LG, the MG-LG boundary, the same time step cannot be used for the advection. In this study, the update procedure is performed as follows. The first of all, the variables are updated from n to the intermediate situation $*$, then they are updated to $n+\frac{1}{2}$. Similarly, they are done from $n+\frac{1}{2}$ to $**$, and then to $n+1$. Suppose the LG is spaned over $i_1\le i\le i_2$ and $j_1\le j\le j_2$. The update

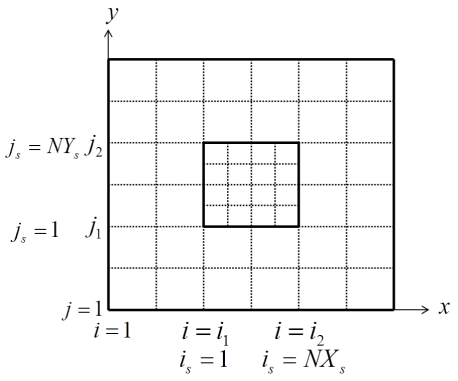

Fig. 2. The main and the local grids and their coodinate indeces

equations are given as follows.

$$f_x^{+,*}(i_1,j) = A_{x1}^{+,t} f_x^{+,n}(i_1,j) + A_{x2}^{+,t} f_x^{+,n}(i_1-1,j) + A_{x3}^{+,t} g_x^{+,n}(i_1,j) + A_{x4}^{+,t} g_x^{+,n}(i_1-1,j) \quad (25)$$

$$g_x^{+,*}(i_1,j) = B_{x1}^{+,t} g_x^{+,n}(i_1,j) + B_{x2}^{+,t} g_x^{+,n}(i_1-1,j) + B_{x3}^{+,t} f_x^{+,n}(i_1,j) + B_{x4}^{+,t} f_x^{+,n}(i_1-1,j) \quad (26)$$

$$\eta_x^{+,*}(i_1,j) = C_{x1}^{+,t} \eta_x^{+,n}(i_1,j) + C_{x2}^{+,t} \eta_x^{+,n}(i_1-1,j) \quad (27)$$

$$f_x^{+,**}(i_1,j) = A_{x1}^{+,T} f_x^{+,n}(i_1,j) + A_{x2}^{+,T} f_x^{+,n}(i_1-1,j) + A_{x3}^{+,T} g_x^{+,n}(i_1,j) + A_{x4}^{+,T} g_x^{+,n}(i_1-1,j) \quad (28)$$

$$g_x^{+,**}(i_1,j) = B_{x1}^{+,T} g_x^{+,n}(i_1,j) + B_{x2}^{+,T} g_x^{+,n}(i_1-1,j) + B_{x3}^{+,T} f_x^{+,n}(i_1,j) + B_{x4}^{+,T} f_x^{+,n}(i_1-1,j) \quad (29)$$

$$\eta_x^{+,**}(i_1,j) = C_{x1}^{+,T} \eta_x^{+,n}(i_1,j) + C_{x2}^{+,T} \eta_x^{+,n}(i_1-1,j) \quad (30)$$

$$f_x^{-,*}(i_2,j) = A_{x1}^{-,t} f_x^{-,n}(i_2,j) + A_{x2}^{-,t} f_x^{-,n}(i_2+1,j) + A_{x3}^{-,t} g_x^{-,n}(i_2,j) + A_{x4}^{-,t} g_x^{-,n}(i_2+1,j) \quad (31)$$

$$g_x^{-,*}(i_2,j) = B_{x1}^{-,t} g_x^{-,n}(i_2,j) + B_{x2}^{-,t} g_x^{-,n}(i_2+1,j) + B_{x3}^{-,t} f_x^{-,n}(i_2,j) + B_{x4}^{-,t} f_x^{-,n}(i_2+1,j) \quad (32)$$

$$\eta_x^{-,*}(i_2,j) = C_{x1}^{-,t} \eta_x^{-,n}(i_2,j) + C_{x2}^{-,t} \eta_x^{-,n}(i_2+1,j) \quad (33)$$

$$f_x^{-,**}(i_2,j) = A_{x1}^{-,T} f_x^{-,n}(i_2,j) + A_{x2}^{-,T} f_x^{-,n}(i_2+1,j) + A_{x3}^{-,T} g_x^{-,n}(i_2,j) + A_{x4}^{-,T} g_x^{-,n}(i_2+1,j) \quad (34)$$

$$g_x^{-,**}(i_2,j) = B_{x1}^{-,T} g_x^{-,n}(i_2,j) + B_{x2}^{-,T} g_x^{-,n}(i_2+1,j) + B_{x3}^{-,T} f_x^{-,n}(i_2,j) + B_{x4}^{-,T} f_x^{-,n}(i_2+1,j) \quad (35)$$

$$\eta_x^{-,**}(i_2,j) = C_{x1}^{-,T} \eta_x^{-,n}(i_2,j) + C_{x2}^{-,T} \eta_x^{-,n}(i_2+1,j) \quad (36)$$

IV. Numerical results

In order to verify the validity of the spatial and the temporal interpolations, we compare the numerical results with and without the interpolations.

A. Numerical results of the spatial interpolation

Fig. 3 shows the computational region $R_x = R_y = 1$ m of the free space, with the subgrid region $0.4 \le x \le 0.6, 0.5 \le y \le 0.7$. The cell size of the main grids is $\Delta X = \Delta Y = 1 \times 10^{-2}$ m, and the one of the local grids is $\Delta x = \Delta x = 5 \times 10^{-3}$ m.

The time step Δt [s] is chosen as $\Delta t = \frac{0.5}{c_0\sqrt{\Delta x^{-2}+\Delta y^{-2}}}$. The line current at $x = 0.5, y = 0.2$ m excites the fields with the waveform:

$$J_z = \begin{cases} \frac{1}{\Delta x \Delta y}\sin^3(\omega t), & (0 \le t < \frac{2\pi}{\omega}) \\ 0, & (t < 0, t > \frac{2\pi}{\omega}) \end{cases}, \quad (37)$$

where $\omega = 2\pi f_c$ rad/s, and $f_c = 5 \times 10^8$ Hz.

The observation points A and B are set at $(x,y) = (0.5, 0.4), (0.5, 0.8)$, and the results are compared with the ones computated by the uniform cell size $\Delta x = \Delta y = 5 \times 10^{-3}$ m.

Fig. 4 shows the observed waveform of e_z at the points A and B, and their frequency characteristics are shown in Fig. 5.

As we can see from Fig. 4, the results with and without the subgrids agree well with each other, therefore we can say no spurious reflection caused by the MG-LG boundary. Moreover, the late time instability does not occur in the numerical experiments.

In Fig. 5, the results agree with each other in the lower frequency band, but some discrepancies are found in the higher frequency band. It is expected that the discrepancies are caused by the insufficient sampling in the main grids.

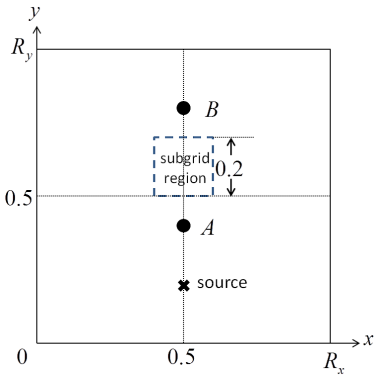

Fig. 3. The configuration used in the numerical verification

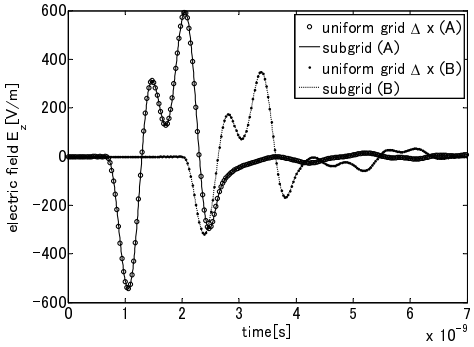

Fig. 4. The observed waveform at A and B

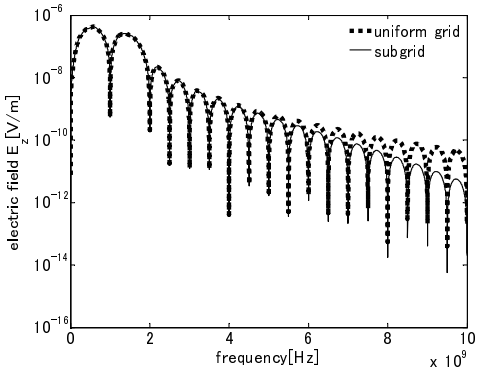

Fig. 5. The amplitude of the frequency characteristics at the observation point A

B. Numerical results of the temporal interpolation

In order to examine the validity of the proposed temporal interpolation, we perform the numerical experiment in the computation region with $R_x = R_y = 1$ m as shown in Fig. 3. The cell size is $\Delta X = \Delta Y = 1 \times 10^{-2}$ m. The LG region is set in $0.5 \leq x \leq 0.7, 0 \leq y \leq R_y$.

The time step in the MG, ΔT, is taken as $\Delta T = \frac{0.5}{c_0\sqrt{\Delta x^{-2}+\Delta y^{-2}}}$ and in the LG, $\Delta t = \frac{\Delta T}{2}$. The same line current as the previous section is used to excite fields. We observe the fields at $(x, y) = (0.4, 0.5)$, and $(0.8, 0.5)$, and compare with the results using only ΔT in the entire region.

The waveforms observed at the observation points are plotted in Fig. 7, and the amplitude of the spectra are shown in Fig. 8.

In Fig. 7, the results with and without the temporal interpolation agree well with each other, and no spurious fields caused by the interpolation are observed. In Fig. 8, the results coincides with each other, and the relative error at the frequency $f_c = 5 \times 10^8$ Hz is about 0.01 %-0.3 %. Therefore the spatial and the temporal interpolations proposed in this study operate with high precision.

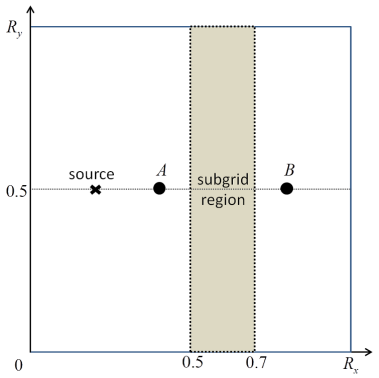

Fig. 6. Configuration for numerical examination

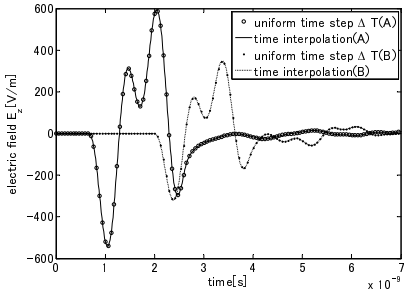

Fig. 7. The waveforms obtained at the observation points

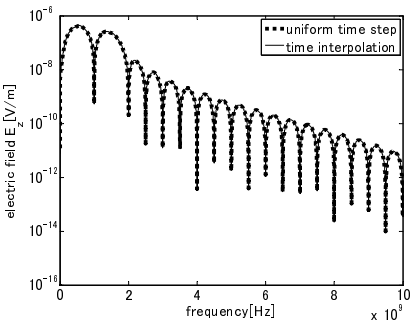

Fig. 8. The spectrum at the point A

V. Conclusion

In this study, we develop the subgridding technique for the CIP method in order to analyze fine structures with low computational costs. The subgridding technique consists of the spatial and the temporal interpolations, and the both are developed separately. The numerical results have shown that the proposed techniques operate well with high precision over wide frequency range.

The future work is to use both the interpolation simultaneously to apply the subgridding approach to practical problems, such as scattering from objects with smooth surface.

Appendix

The coefficients for the update equations are given as follows.

$$A_{\alpha 1}^{\pm,\beta} = 1 - 3\xi^2 + 2\xi^3 \quad \text{(A.1)}$$
$$A_{\alpha 2}^{\pm,\beta} = 3\xi^2 - 2\xi^3 \quad \text{(A.2)}$$
$$A_{\alpha 3}^{\pm,\beta} = \pm\Delta\alpha(-\xi + 2\xi^2 - \xi^3) \quad \text{(A.3)}$$
$$A_{\alpha 4}^{\pm,\beta} = \pm\Delta\alpha(\xi^2 - \xi^3) \quad \text{(A.4)}$$
$$B_{\alpha 1}^{\pm,\beta} = 1 - 4\xi + 3\xi^2 \quad \text{(A.5)}$$
$$B_{\alpha 2}^{\pm,\beta} = -2\xi + 3\xi^2 \quad \text{(A.6)}$$
$$B_{\alpha 3}^{\pm,\beta} = \pm\frac{6}{\Delta\alpha}(\xi - \xi^2) \quad \text{(A.7)}$$
$$B_{\alpha 4}^{\pm,\beta} = -B_{\alpha 3}^{\pm} \quad \text{(A.8)}$$
$$C_{\alpha 1}^{\pm,\beta} = 1 - \xi \quad \text{(A.9)}$$
$$C_{\alpha 2}^{\pm,\beta} = \xi \quad \text{(A.10)}$$

where

$$\xi = \frac{c\Delta\beta}{\Delta\alpha} \quad \text{(A.11)}$$
$$\alpha = x, y \quad \text{(A.12)}$$
$$\beta = t, T \quad \text{(A.13)}$$

References

[1] T. Yabe, F. Xiao, and T. Utsumi, "The constrained interpolation profile method for multiphase analysis," J. Comp. Phys., vol. 169, pp. 556-593, 2001.

[2] Y. Ando and M. Hayakawa, "Implementation of the perfect matched layer to the CIP method," IEICE Trans. Electron., vol. E89-C, no. 5, pp. 645-648, 2006.

[3] Y. Ando and S. Murakoshi, "A total-field/scattered-field boundary for the multi-dimensional CIP method," IEICE Trans. Electron., vol. E95-C, no. 1, pp. 115-121, 2012.

[4] A. Taflove and S. C. Hangness, *Computational Electrodynamics*, Artech House, 2000.

[5] T. Yabe, H. Mizoe, K. Takizawa, H. Moriki, H. N. Im, and Y. Ogata, "Higher-order schemes with CIP method and adaptive Soroban grid towards mesh-free scheme," J. Comp. Phys., vol. 194, pp. 57-77, 2004.

[6] K. Xiao, D. J. Pommerenke, and J. L. Drewniak, "A three-dimensional FDTD subgridding algorithm with separeted temporal and spatial interfaces and related stability analysis," IEEE Trans. Antennas Propagat., vol. 55, no. 7, pp. 1981-1990, 2007.